Characterization of meningeal type 2 innate lymphocytes and their response to CNS injury

Sachin P. Gadani,[1,2,3,4] Igor Smirnov,[1,2] Ashtyn T. Wiltbank,[1,2,3] Christopher C. Overall,[1,2] and Jonathan Kipnis[1,2,3,4]

[1]Center for Brain Immunology and Glia (BIG), [2]Department of Neuroscience, [3]Graduate Program in Neuroscience, and [4]Medical Scientist Training Program, University of Virginia, Charlottesville, VA 22908

The meningeal space is occupied by a diverse repertoire of immune cells. Central nervous system (CNS) injury elicits a rapid immune response that affects neuronal survival and recovery, but the role of meningeal inflammation remains poorly understood. Here, we describe type 2 innate lymphocytes (ILC2s) as a novel cell type resident in the healthy meninges that are activated after CNS injury. ILC2s are present throughout the naive mouse meninges, though are concentrated around the dural sinuses, and have a unique transcriptional profile. After spinal cord injury (SCI), meningeal ILC2s are activated in an IL-33–dependent manner, producing type 2 cytokines. Using RNAseq, we characterized the gene programs that underlie the ILC2 activation state. Finally, addition of wild-type lung-derived ILC2s into the meningeal space of IL-33R$^{-/-}$ animals partially improves recovery after SCI. These data characterize ILC2s as a novel meningeal cell type that responds to SCI and could lead to new therapeutic insights for neuroinflammatory conditions.

The Journal of Experimental Medicine

INTRODUCTION

The healthy central nervous system (CNS) parenchyma is void of resident immune cells besides microglia. However, there is a full repertoire of resident immune cells, including macrophages, T cells, and B cells, in the meningeal spaces. Meningeal leukocytes support normal brain function (Derecki et al., 2010; Filiano et al., 2016), can drain to local lymph nodes (Louveau et al., 2015), and present autoantigens in the context of experimental autoimmune encephalomyelitis (EAE; Kivisäkk et al., 2009), but their activation and role after CNS injury are poorly understood.

Injury to the CNS is devastating and often results in profound impairment caused by lack of regeneration and secondary neuronal death, the progressive loss of neurons not injured by the primary insult (Dusart and Schwab, 1994). A prominent feature of CNS injury is the immune response that starts rapidly and has distinct beneficial effects on outcome, largely through its effect on secondary neuronal damage (Shechter et al., 2009; Gadani et al., 2015a). The inflammatory cascade begins with release of alarm signals (alarmins) that initiate a cellular response. We have previously characterized the protein IL-33 as a key CNS alarmin that is expressed in healthy glia, is released after injury, and promotes monocyte recruitment (Gadani et al., 2015b).

Interestingly, IL-33 is released into the cerebrospinal fluid (CSF) after spinal cord injury (SCI; Gadani et al., 2015b), leading to the possibility of it activating meningeal cells there. Type 2 innate lymphocytes (ILC2s) are recently described tissue-resident cells (Moro et al., 2010; Neill et al., 2010; Price et al., 2010; Molofsky et al., 2013) and are among the most potent responders to IL-33 in the periphery. Upon interaction with IL-33, ILC2s rapidly produce cytokines such as IL-13 and IL-5, initiating and potentiating type 2 immunity (Van Dyken et al., 2014). In the periphery, ILC2s are important mediators of antihelminth and allergic inflammation (Halim, 2016) and promote healing in skin (Rak et al., 2016) and lung (Monticelli et al., 2011) injury models. ILC2s have previously been detected in the CNS, where they are responsible for gender differences in the EAE response of male and female *Kit* mutant mice (Russi et al., 2015), but their presence in the meninges and response to CNS injury has not been studied.

Here, we identify ILC2s as a novel meninges-resident cell type and characterize their localization, transcriptional profile, and response to CNS injury. Meningeal ILC2s are concentrated around the dural sinuses and have unique transcriptional profiles and basal activation states when compared with peripheral (lung) ILC2s. Meningeal ILC2s are activated in an IL-33–dependent manner after CNS injury. Finally, addition of WT lung-derived ILC2s into CSF of IL-33R$^{-/-}$ mice before injury improves functional outcome and reduces lesion size after SCI, suggesting that these cells play a beneficial post–CNS injury role.

Correspondence to Sachin P. Gadani: sg8th@virginia.edu; or Jonathan Kipnis: kipnis@virginia.edu

Abbreviations used: BMS, Basso mouse scale; CGRP, calcitonin gene-related peptide; CNS, central nervous system; CSF, cerebrospinal fluid; ILC2, type 2 innate lymphocyte; SCI, spinal cord injury.

The Rockefeller University Press $30.00
J. Exp. Med. 2017 Vol. 214 No. 2 285–296
https://doi.org/10.1084/jem.20161982

RESULTS AND DISCUSSION

The meningeal compartment of the CNS hosts a wide variety of immune cells under homeostatic conditions. ILC2s, known for their important functions in barrier tissues, had previously been implicated in CNS diseases (Besnard et al., 2015; Russi et al., 2015), but their presence in healthy meninges has not been assessed. We asked whether ILC2s are present in healthy meninges and surprisingly identified a population of $CD45^+/Lineage^-/Thy1.2^+/ST2^+$ cells (Fig. 1 A). Furthermore, this population had a surface marker profile characteristic of ILC2s, expressing C-kit, Sca1, CD25, and IL-7Rα (Fig. 1 B). Interestingly, the meninges has more ILC2s relative to ILC3s ($CD45^+$/singlets/$lineage^-$/viable/$ROR\gamma^+$ cells) in the healthy state, and both ILC populations were concentrated in the brain rather than spinal cord meninges (Fig. 1 C). No ILCs were detected in the healthy spinal cord parenchyma (Fig. 1 C).

We next sought to explore the physical localization of ILC2s in brain and spinal cord meninges. To that end, we crossed the Yet-Cre 13 (Price et al., 2010) and $tdTomato^{stoplox}$ mice, generating a new model where any cell that expressed IL-13 is permanently labeled with tdTomato ($IL\text{-}13^{tdt}$ mice). This strategy labels the majority of ILC2s in healthy brain/spinal cord meninges and lung (Fig. 1, D and E) and also labels populations of T cells and mast cells in these tissues (Fig. 1, F and G). A whole mount of $IL\text{-}13^{tdt}$ dura mater revealed a concentration of tdTomato expression in the transverse and sagittal dural sinuses, which drain venous blood from the brain (Fig. S1 A). To differentiate $tdTomato^+$ ILC2s from T cells and mast cells, we costained $IL\text{-}13^{tdt}$ meninges with CD3 and toluidine blue to identify T cells and mast cells, respectively. ILC2s were identified as $tdTomato^+/CD3^-$/toluidine $blue^-$ cells in dural sinus, dura mater, and spinal cord meninges whole mounts (Fig. 1, H–J). ILC2s were heavily concentrated in the dural sinus and found more sparsely throughout the dura mater and spinal cord meninges (Fig. 1 K).

It has previously been noted that ILC2s expand in response to IL-33 stimulation (Molofsky et al., 2013), and, to further confirm the nature of the newly identified meningeal cells, we sought to repeat this observation in meningeal ILC2s. Indeed, mice treated with IL-33 i.p. for 6 d had up to 3.5-fold expansion of ILC2s in the spinal cord and brain meninges (Fig. 1, L–N).

Given the unique localization of brain meningeal ILC2s, we characterized them transcriptionally to assess their degree of similarity with other ILC2s, choosing to compare them with the well-studied population of ILC2s in the lung. ILC2s were FACs purified from meninges and lung, and >90% pure ILC2s were used for RNAseq analysis. Among the top genes expressed by meningeal ILC2s are numerous canonical markers, including the *Il-2rα*, *Il-7r*, and *Il1rl1* (IL-33R; Fig. 2 A and Table S1). To assess the similarity of highly expressed genes in meningeal and lung ILC2s, we compared the genes expressed at least 1.5 standard deviations above the mean between the cell types. As predicted, the majority of highly expressed genes are common between lung and meningeal ILC2s, but there are also discreet sets of genes delineating them (Fig. 2 B). We identified 472 significantly altered genes between the groups (adjusted p-value <0.05; Fig. 2 C and Table S2). Interestingly, the majority of these genes were up-regulated in lung relative to meningeal ILC2s (Fig. 2 C). To describe functional consequences of this differential expression, we identified gene sets enriched among our differentially expressed genes (Table S2). Among the enriched gene sets were several relating to inflammation, signal transduction, and metabolism, suggesting an increased basal activation state in lung relative to meningeal ILC2s (Fig. 2, D and E). The basis for these differences is somewhat unclear. Lung ILC2s are exposed to far more environmental irritants and stimuli than meningeal ILC2s, likely leading to the observed alternations in transcription. Furthermore, meningeal ILC2s are proximal to the brain, an exceptionally sensitive tissue, and therefore, a relatively quiescent rest state could be optimal for healthy brain function.

IL-33 is a potent stimulus for ILC2s and is released in abundance into the CSF after SCI (Gadani et al., 2015b). We therefore tested whether meningeal ILC2s are acutely activated after SCI. Type 2 cytokine production is a hallmark of ILC2 activation, and using the YET-cre 13 mouse (which have YFP expressed under the IL-13 promoter), we compared IL-13 induction in uninjured and 1 d post-injury (1DPI) ILC2s, finding increased YFP expression in brain but not spinal cord meningeal ILC2s (Fig. 3 A). We repeated this observation using intracellular antibody staining, finding that brain meningeal but not spinal cord meningeal ILC2s have increased production of IL-13 and IL-5 at 1DPI (Fig. 3, B and C). Finally, we tested whether brain meningeal ILC2 cytokine production is IL-33 dependent using the $IL\text{-}33^{-/-}$ mice. $IL\text{-}33^{-/-}$ animals show no significant up-regulation of IL-13 or IL-5 relative to uninjured animals (Fig. 3, D and E).

Brain meningeal ILC2s respond to spinal cord–derived signals after injury with increased cytokine production, and we next characterized the transcriptome of SCI-activated meningeal ILC2s by RNAseq. We measured global transcriptomic changes in brain meningeal ILC2s 1 d after SCI, finding numerous up- and down-regulated genes (Fig. 3 F and Table S3). Among genes up-regulated after injury are immune checkpoint genes, such as *Pdcd1*, receptors, such as *Tnfrsf9*, *Gpr35*, and *Il18r1*, and those involved in neuroprotection, such as *Calca* (encoding calcitonin gene-related peptide [CGRP]) and the shuttle for its receptor *Ramp3* (Fig. 3 F). CGRP is known to be rapidly up-regulated in the injured CNS (Bulloch et al., 1998; Ackery et al., 2007) and is involved in regeneration of peripheral nerves (Blesch and Tuszynski, 2001; Toth et al., 2009). Notably, expression of *Il1rl1* (encoding ST2), *Il5*, and *Il13* were unchanged after injury. The lack of measured difference in IL-5 and IL-13 mRNA could represent the transient nature of their up-regulation in this system. Although the Yet-cre reporter demonstrated increased YFP, and thus IL-13 promoter activity at

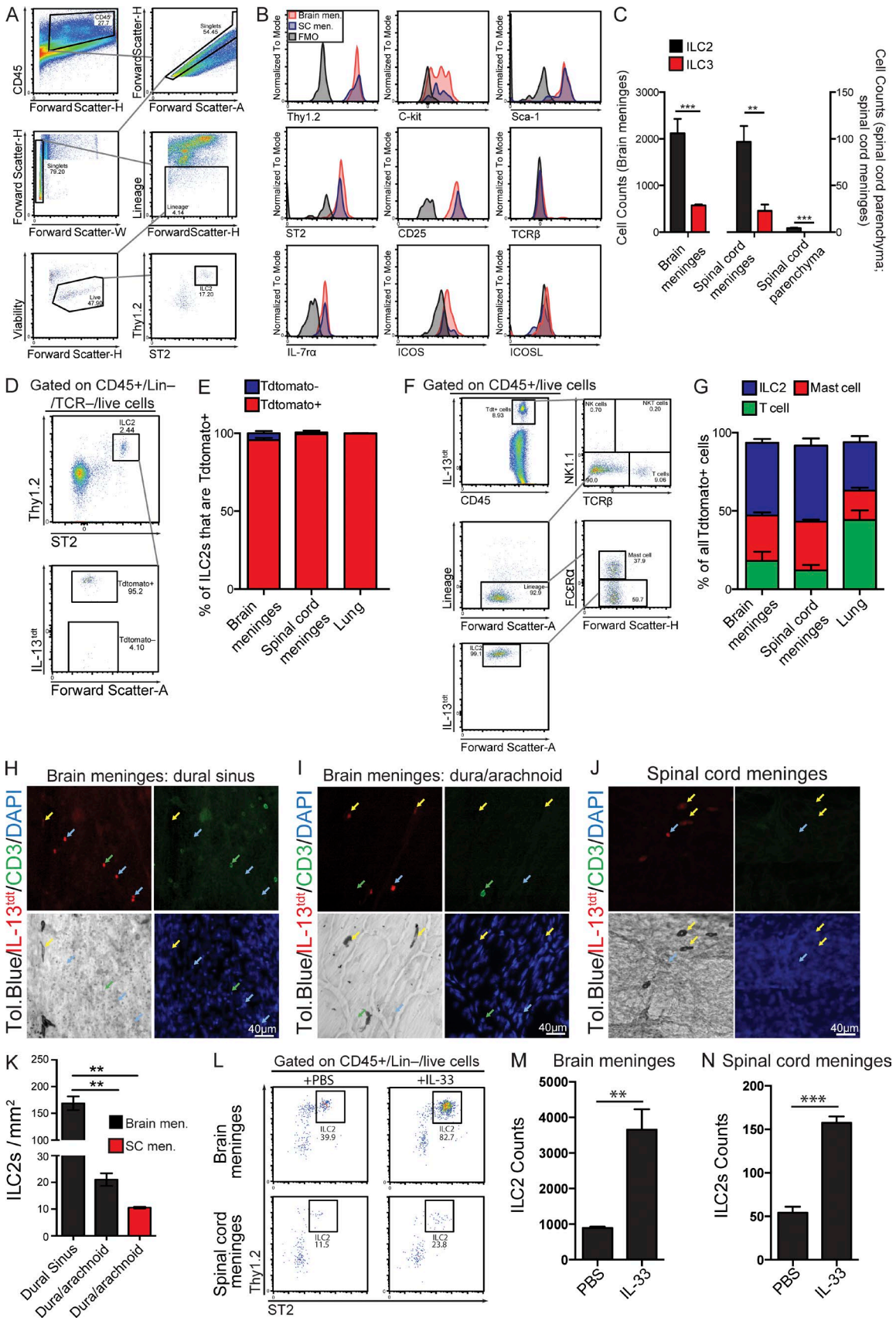
A
CD45
Forward Scatter-H
Forward Scatter-A
Forward Scatter-W
Lineage
Viability
Thy1.2
ST2
B
Brain men.
SC men.
FMO
Normalized To Mode
Thy1.2
C-kit
Sca-1
ST2
CD25
TCRβ
IL-7rα
ICOS
ICOSL
C
ILC2
ILC3
Cell Counts (Brain meninges)
Cell Counts (spinal cord parenchyma; spinal cord meninges)
Brain meninges
Spinal cord meninges
Spinal cord parenchyma
D
Gated on CD45+/Lin–/TCR–/live cells
IL-13tdt
Tdtomato+
Tdtomato–
E
Tdtomato-
Tdtomato+
% of ILC2s that are Tdtomato+
Brain meninges
Spinal cord meninges
Lung
F
Gated on CD45+/live cells
NK cells
NKT cells
T cells
Mast cell
Lineage
FCεRα
G
ILC2
Mast cell
T cell
% of all Tdtomato+ cells
H
Brain meninges: dural sinus
I
Brain meninges: dura/arachnoid
J
Spinal cord meninges
Tol.Blue/IL-13tdt/CD3/DAPI
40μm
K
ILC2s / mm2
Brain men.
SC men.
Dural Sinus
Dura/arachnoid
L
Gated on CD45+/Lin–/live cells
+PBS
+IL-33
Brain meninges
Spinal cord meninges
M
Brain meninges
ILC2 Counts
PBS
IL-33
N
Spinal cord meninges
ILC2s Counts

1DPI, it is possible that increases in IL-13 mRNA are outlived by the YFP reporter.

We next identified gene sets enriched in meningeal ILC2s isolated from uninjured versus injured mice. Several inflammatory gene networks were enriched in ILC2s after injury, including TNF signaling, IL-2 signaling, biosynthetic processes, and general cell activation (Fig. 3, G and H; and Table S3). Interestingly, several of the same genes and gene sets were up-regulated in meningeal ILC2s after injury and lung ILC2s. Extracting sufficient RNA for analysis from meningeal ILC2s required pooling five mice per sample, and we therefore chose to validate results using RNAseq replicates instead of individual gene qPCR. RNAseq replicates were collected on different days, and only genes/gene sets consistently different across samples were accepted.

ILC2s are known to accumulate at injury sites in the periphery (Rak et al., 2016), but the capacity for ILC2 migration into inflamed sites is poorly understood. Given that the healthy CNS parenchyma is void of ILC2s (Fig. 1 C), we reasoned that if ILC2s accumulate at the SCI site, some of them must have migrated there. We used the IL-13^{tdt} mouse to identify ILC2s that have infiltrated the lesion site, finding that they migrate to the injury site by 10DPI (Fig. 4 A). Using flow cytometry, we performed a time course of ILC2 numbers in the SCI site. ILC2s were detectable in the injury site by 3DPI, but numbers maximized at 10DPI and persisted through 30DPI (Fig. 4 B). Notably, these cells were competent to produce IL-13 (Fig. 4 C). This migration was IL-33 independent, as IL-33$^{-/-}$ and WT mice had similar ILC2 infiltration at 10DPI (Fig. 4 D).

Finally, we sought to test the functional impact ILC2s have on recovery from CNS injury. We pursued a global ILC depletion strategy: Rag1$^{-/-}$ animals, lacking T and B cells but having Thy1.2^{+} ILCs, were reconstituted with Thy1.1 lymphocytes. In this mouse, reconstituted lymphocytes will bear a different isoform Thy1 than endogenous ILCs. We then injected mice with a Thy1.2-depleting antibody, targeting ILCs without affecting lymphocytes, as had been previously performed in literature (Monticelli et al., 2011; Gorski et al., 2013). There was no significant effect of depleting ILCs in this way on SCI outcome (Fig. S2 A); however, the depletion strategy was actually found to be ineffective for meninges. Anti-Thy1.2 did not deplete meningeal ILCs, but instead only blocked the Thy1 epitope (Fig. S2, B and C). Our observation should also serve as a caution against validating depletion by staining for the antigen used to deplete.

We next pursued the converse experiment: adding back ILC2s into the CSF before injury. Meningeal ILC2s are sparse, and it is not feasible to extract sufficient numbers for reconstitution. Given their relative abundance and increased basal activity profiles, we used lung-derived ILC2s for adoptive transfer experiments. ILC2 cytokine production is dependent on IL-33, and to restrict IL-33's actions only to our transferred cells, we used ST2$^{-/-}$ recipients. 5,000 FACS-purified, lung-derived ILC2s were injected into the cisterna magna of ST2$^{-/-}$ mice 1 d before SCI. This moderate increase in ILC2 numbers had a significant beneficial effect on functional recovery, as measured by Basso mouse scale (BMS) score, a behavior score widely used to assess functional outcome of SCI in mice (Fig. 4 E). Additionally, we measured the volume size of the lesions, and as expected from BMS scores, ILC2-treated mice had smaller lesion volumes than control mice (Fig. 4, F and G). Lung ILC2s were selected based on their availability and activation profile, which includes elevated immunomodulatory and neuroprotective gene expression. It is important to realize that in using these cells, we may have tilted the balance in favor of recovery and that reconstitution with more meningeal ILC2s would be required to achieve the same benefit. Alternatively, meningeal ILC2s may be specialized to support the injured CNS through unidentified mechanisms, in which case our reconstitution underestimates the true impact of ILC2s on SCI.

The meningeal space represents a largely unstudied venue for neuroimmune interactions in the healthy and diseased CNS conditions. This area is densely populated by a variety of immune cells, some resident (Goldmann et al., 2016)

Figure 1. **ILC2s are meningeal-resident cells concentrated around the dural sinus.** (A) Representative gating of meningeal ILC2s. ILC2s were identified by flow cytometry as CD45^{+}/singlets/lineage^{-}/viable/ST2^{+}/CD25^{+} cells (Lineage cocktail = CD11b, GR1, CD3, B220, FcεRα, Ter-119; representative of three biological replicates). (B) Flow cytometry characterization of meningeal ILC2s (representative of three biological replicates). (C) Counts of mouse ILC2s and ILC3s (CD45^{+}/singlets/lineage^{-}/viable/RORγt^{+} cells) in healthy mouse brain meninges (P = 0.007; left y axis), spinal meninges (P = 0.015), and spinal cord parenchyma (P = 0.002; right y axis; *n* = 3; multiple Student's *t* tests). (D–G) Characterization of the IL-13^{tdt} mouse by flow cytometry. (D) Representative flow plots of ILC2 tdTomato expression. Lineage cocktail omitted anti-FcεRα in D and F to allow separate visualization. (E) >95% of ILC2s are tdTomato^{+} in IL-13^{tdt} mouse brain and spinal cord meninges and lung (*n* = 3; representative of three experiments). (F) Representative flow plots of tdTomato expression of other meningeal cell types. (G) ILC2s, T cells, and mast cells account for the majority of total tdTomato^{+} cells in brain and spinal cord meninges and lung (*n* = 3; representative of two experiments). (H–J) Representative images of ILC2s identified as IL-13^{tdt}+/CD3^{-}/toluidine blue^{-} cells in dural sinus (H), dura/arachnoid mater (I), or spinal cord meninges (J) whole mounts (blue arrows represent IL-13^{tdt}+/CD3^{-}/toluidine blue^{-} ILC2s, green arrows represent IL-13^{tdt}+ or −/CD3^{-}/toluidine blue^{-} T cells, and yellow arrows represent IL-13^{tdt}+/CD3^{-}/toluidine blue^{+} mast cells). (K) Quantification of ILC2 localization demonstrates a concentration in the dural sinus versus other meninges areas (P < 0.0001; *n* = 3–4; one-way ANOVA with Tukey's multiple comparisons test). (L–N) Mice were treated with IL-33 every other day for 6 d i.p., and on the eighth day, ILC2 numbers were analyzed by flow cytometry. (L) Representative plots demonstrating expansion of ILC2s in IL-33–treated mice relative to PBS treatment (gated on live/CD45^{+}/singlet/Lineage^{-} cells). (M and N) Counts demonstrating expansion in brain meninges (M; P = 0.009) and spinal cord meninges (N; P = 0.001; *n* = 3, representative of three experiments; Student's *t* test). Error bars represent mean ± SEM; **, P ≤ 0.01; ***, P ≤ 0.001.

A

	Symbol	Name	Entrez ID
1	COX1	cytochrome c oxidase subunit I	17708
2	Malat1	metastasis associated lung adenocarcinoma transcript 1 (non-coding RNA)	72289
3	Xist	inactive X specific transcripts	213742
4	CYTB	cytochrome b	17711
5	Macf1	microtubule-actin crosslinking factor 1	11426
6	B2m	beta-2 microglobulin	12010
7	ND5	NADH dehydrogenase subunit 5	17721
8	Lars2	leucyl-tRNA synthetase, mitochondrial	102436
9	**Il1rl1**	**interleukin 1 receptor-like 1**	**17082**
10	Serinc3	serine incorporator 3	26943
11	Inpp4b	inositol polyphosphate-4-phosphatase, type II	234515
12	Actb	actin, beta	11461
13	Prrc2c	proline-rich coiled-coil 2C	226562
14	Mbnl1	muscleblind-like 1 (Drosophila)	56758
15	ND4	NADH dehydrogenase subunit 4	17719
16	Eef1a1	eukaryotic translation elongation factor 1 alpha 1	13627
17	Srrm2	serine/arginine repetitive matrix 2	75956
18	Ptprc	protein tyrosine phosphatase, receptor type, C	19264
19	Dock10	dedicator of cytokinesis 10	210293
20	Aff4	AF4/FMR2 family, member 4	93736
21	ND1	NADH dehydrogenase subunit 1	17716
22	Ccr2	chemokine (C-C motif) receptor 2	12772
23	**Il7r**	**interleukin 7 receptor**	**16197**
24	**Il2ra**	**interleukin 2 receptor, alpha chain**	**16184**
25	H2-K1	histocompatibility 2, K1, K region	14972
26	Ddx5	DEAD (Asp-Glu-Ala-Asp) box polypeptide 5	13207
27	Cnot6l	CCR4-NOT transcription complex, subunit 6-like	231464
28	Msn	moesin	17698
29	Huwe1	HECT, UBA and WWE domain containing 1	59026
30	Itga4	integrin alpha 4	16401
31	Samhd1	SAM domain and HD domain, 1	56045
32	Son	Son DNA binding protein	20658
33	Ikzf1	IKAROS family zinc finger 1	22778
34	Kmt2c	lysine (K)-specific methyltransferase 2C	231051
35	Lcp1	lymphocyte cytosolic protein 1	18826
36	Mdfic	MyoD family inhibitor domain containing	16543
37	Ncor1	nuclear receptor co-repressor 1	20185
38	Ahnak	AHNAK nucleoprotein (desmoyokin)	66395
39	Kmt2a	lysine (K)-specific methyltransferase 2A	214162
40	Mycbp2	MYC binding protein 2	105689
41	Birc6	baculoviral IAP repeat-containing 6	12211
42	Ywhaz	tyrosine 3-monooxygenase/tryptophan 5-monooxygenase activation protein, zeta polypeptide	22631
43	Smg1	SMG1 homolog, phosphatidylinositol 3-kinase-related kinase (C. elegans)	233789
44	ND2	NADH dehydrogenase subunit 2	17717
45	Ahcyl2	S-adenosylhomocysteine hydrolase-like 2	74340
46	Ube2d3	ubiquitin-conjugating enzyme E2D 3	66105
47	Tmsb4x	thymosin, beta 4, X chromosome	19241
48	Stab2	stabilin 2	192188
49	Mdm4	transformed mouse 3T3 cell double minute 4	17248
50	Aak1	AP2 associated kinase 1	269774

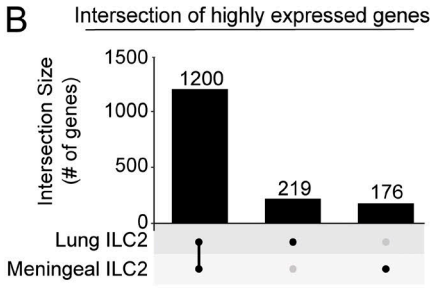

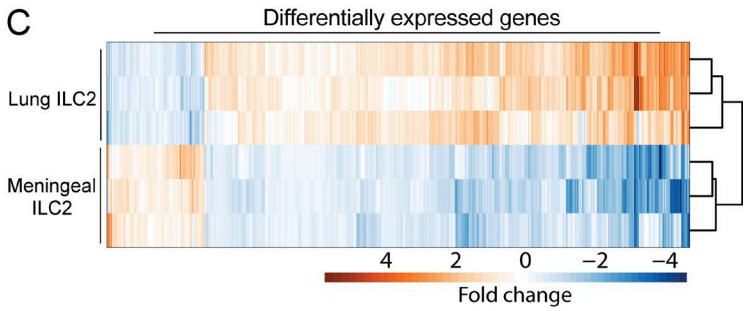

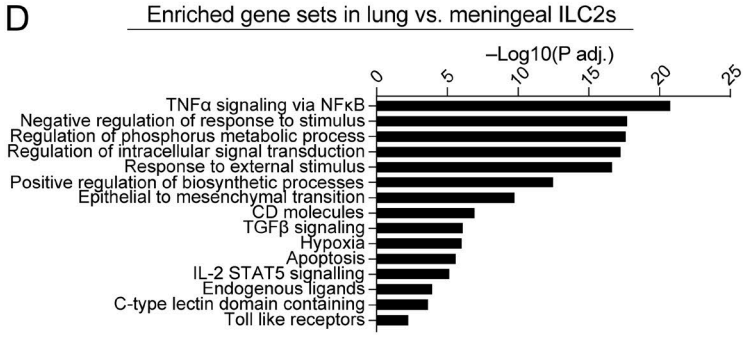

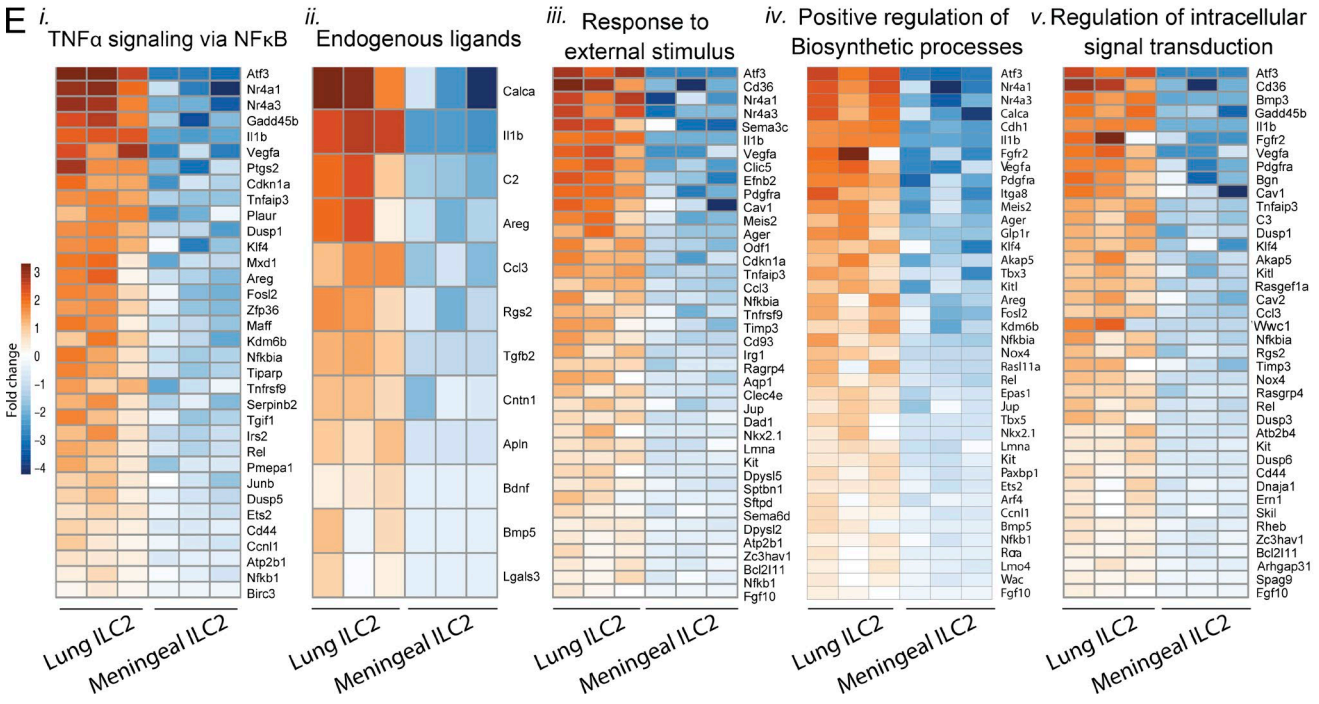

and other patrolling (Radjavi et al., 2014). The recent discovery of meningeal lymphatic vessels (Aspelund et al., 2015; Louveau et al., 2015) has shed a new light on the importance of the meningeal space in the neuroimmune axis. Meningeal immunity is unique as it exhibits an obvious predominance of type 2 inflammation (Derecki et al., 2010) for reasons that are not fully understood yet. Moreover, after SCI, type 2 immune responses are intensified and required for improved outcome (Walsh et al., 2015). One of the immediate cells responding to injuries in peripheral/barrier tissues are ILC2s. Here, we provide the first evidence for a meningeal population of ILC2s, demonstrating their abundance in the brain meninges and characterizing them transcriptionally. We further studied their response to SCI, demonstrating that after injury, meningeal ILC2s are functionally activated, and they enter the injury site and improve recovery.

Our finding of differential gene expression from brain and lung further suggests that ILC2 phenotype could be determined, at least in part, by tissue of residence. Indeed, diverse tissue-dependent ILC2 functions have already been described in tissues such as adipose (Molofsky et al., 2013; Odegaard et al., 2016). Of note, lung ILC2s had up-regulation of numerous inflammatory gene sets relative to meninges, possibly because of continuous exposure of these cells to environmental irritants and stimuli. The extent of plasticity between and diversity of roles for putative ILC2 phenotypes remains an important topic for future study.

After SCI, meningeal ILC2s are activated, producing type 2 cytokines and up-regulating inflammatory gene sets. Among the most prominently up-regulated genes are *Calca*, encoding CGRP, and *Ramp3*, encoding shuttling protein for its receptor. CGRP is up-regulated in the CNS after injury (Bulloch et al., 1998; Ackery et al., 2007) and has been implicated in regeneration of sensory neurons in and out of the CNS (Blesch and Tuszynski, 2001; Toth et al., 2009), migraine pain (Russo, 2015), and immunomodulation (Bracci-Laudiero et al., 2005). Previous studies have noted CGRP receptor expression in ILC2s, suggesting that they may detect CGRP secreted by nociceptive neurons (Saenz et al., 2013; Talbot et al., 2015). Our results identify CGRP as a novel factor potentially released by activated ILC2s.

This study is an early foray into the biology of meningeal ILC2s and demonstrates a novel role for meningeal immune cells as sentinels for CNS-derived alarmins. IL-33 released after CNS injury not only initiates a local response, but also a meningeal one through actions on ILC2s. ILC2s produce IL-13, both in the meninges and at the injury site, which could promote the generation of neuroprotective Th2 cells—or directly boost survival of neurons (Walsh et al., 2015). Many other potentially neuroprotective factors, including *Areg*, *Vegfa*, *Il1b*, and *Calca* (Blesch and Tuszynski, 2001; Diem et al., 2003; Sun et al., 2003; Zhan et al., 2015) could also contribute to the beneficial effect of lung-derived ILC2 transfer. Further studies are required to fully understand this meningeal ILC2 response and the mechanism by which adding ILC2s is beneficial after injury. Furthermore, meningeal ILC2s, given their perivenous localization, could be first responders in gut–brain communication. This study provides insight into a novel immune cell player after CNS injury, the meningeal ILC2, and further work on this population could lead to therapeutic insights for injury and other neurological disorders.

MATERIALS AND METHODS

Mice

IL-33$^{-/-}$ mice were generated by the trans-NIH Knock-Out Mouse Project (KOMP) and obtained from the KOMP repository. ST2$^{-/-}$ mice were generated in the laboratory of A. McKenzie (University of Cambridge, Cambridge, England, UK) and were a gift from P. Bryce (Northwestern University, Evanston, IL). Yet-Cre 13 mice were generated by and a gift from R. Locksley (University of California, San Francisco, San Francisco, CA; Price et al., 2010). C57/Bl6 and tdTomato^{stoplox} mice were obtained from the Jackson Laboratory, stock #004999 and #007905, respectively. All transgenic lines were on the C57/Bl6 genetic background except for Yet-Cre 13, which was BALB/c. The F1 generation of Yet-Cre 13 × tdTomato^{stoplox} crosses was used. All animals were housed in temperature- and humidity-controlled rooms, maintained on a 12-h light/dark cycle (lights on 7:00 a.m.), and age matched in each experiment. All strains were kept in identical housing conditions. For survival surgeries, mice were anesthetized with either 200 µl of ketamine/xylazine (1 ml ketamine HCl [1 mg/ml], 1 ml of 2% xylazine, 8 ml saline) or inhaled isoflurane. All procedures complied with regulations of the Institutional Animal Care and Use Committee (IACUC) at the University of Virginia (UVA).

Statistics

Statistical tests were performed in Prism (GraphPad Software) or using R as described in the text and figure legends. In all

Figure 2. **RNAseq analysis of ILC2s purified from uninjured meninges and lung.** ILC2s were FACS purified from meninges and lung preparations (DAPI$^-$/CD45$^+$/Lineage$^-$/Thy1.2$^+$/ST2$^+$ cells), and purified mRNA was sequenced on an Illumina platform. (A) The top 50 genes by mean normalized read counts expressed in meningeal ILC2s (n = 3, each sample five pooled mice). (B) UpSet plot comparing highly expressed genes (expressed >1.5 standard deviations above mean) of meningeal and lung ILC2s. 1,200 highly expressed genes were common to both groups, whereas 219 were specific to lung and 176 specific to meningeal ILC2s. (C) Heat map of significantly altered genes between groups (472 genes; n = 3, each sample five pooled mice; adjusted p-value <0.05). (D and E) Gene sets enriched among differentially expressed genes in lung versus meningeal ILC2s. Histogram (D) and heat maps (E) of select gene sets and their component genes (n = 3, each sample five pooled mice; adjusted p-value <0.05).

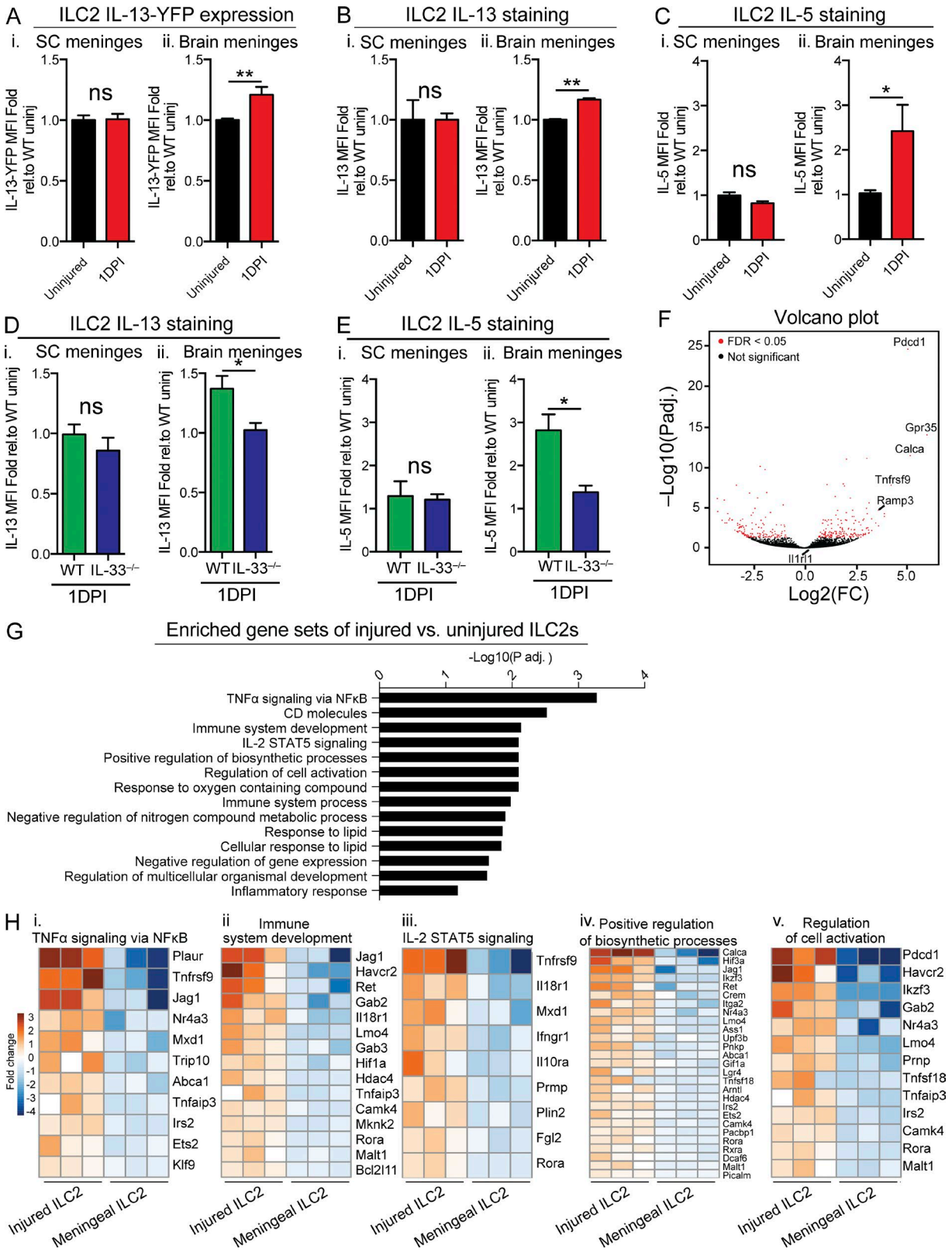

Figure 3. **Activation of meningeal ILC2s after SCI.** (A) ILC2 IL-13 expression assessed by YFP mean fluorescence intensity (MFI) in YET-cre 13 mice in spinal cord (SC) meninges (i; P = 0.890) and brain meninges (ii; P = 0.007; *n* = 9, representative of three pooled experiments; Student's *t* test). (B) Flow cytometry analysis of IL-13 expression in ILC2s at 1DPI in spinal cord meninges (i; P > 0.999) and brain meninges (ii; P < 0.001; *n* = 3, representative of two

figures, error bars represent mean ± SEM; *, P ≤ 0.05; **, P ≤ 0.01; ***, P ≤ 0.001.

Flow cytometry/cell sorting

To prepare single cell suspensions, meninges (brain and spinal cord) were dissected with fine forceps and digested in RPMI + 1.4 U/ml Collagenase VIII (Worthington) + 1 mg/ml DNase1 (Sigma-Aldrich) for 15 min at 37°C. Lungs were dissected, minced, and digested for 30 min in RPMI + 1.4 U/ml Collagenase VIII + 1 mg/ml DNase1 at 37°C. Digested meninges and lung were dissociated by pipetting and passed through 70-µm filters. Spinal cords were dissected from PBS-perfused mice, and 1 cm of cord centered on the lesion was isolated, minced, and digested in RPMI + 4 U/ml papain + 1 mg/ml DNase1 for 20 min. Spinal cords were triturated with small- and large-bore fire-polished pipette and passed through a 70-µm filter. Samples were washed in FACs buffer (PBS, 0.05% Na Azide, 1 mM EDTA, 2% FBS) and stained with antibody cocktail and viability dye for 30 min at 4°C in FACs buffer. For lineage staining, cells were labeled with biotinylated lineage antibody cocktail, washed, and then incubated with strepdavidin-PeCy7 or -Fitc (eBioscience) for 30 min at 4°C. Zombie aqua fixable viability dye (BioLegend) was used to discriminate live cell populations. To obtain absolute cell counts, counting beads (eBioscience) were added to the samples. After staining, samples were washed in FACs buffer and resuspended in 4% PFA. The following antibodies were used (all from eBioscience unless otherwise noted): CD45-af700, Lineage-biotin (CD11b, B220, CD3, GR1, TER-119, FcεRα), Thy1.2-Fitc, ST2-Pe, C-kit–ef780, Sca1-af700, CD25-APC, TCRβ-Fitc or APCCy7, IL-7R–Pe, C-kit–ef7Pe, ICOSL-APC, Gata3-660, Rorγt, IL-13–PeCy7, IL-5–Pe, and CD69-PeCy7.

To stain intranuclear antigens (Gata3, Rorγt, IL-13, IL-5), cells were fixed after extracellular staining with Cytofix/Cytoperm (BD), washed in perm buffer, and stained for 30 min at room temperature. Samples were read on a Gallios cytometer (Beckman Coulter) and analyzed using FlowJo software (Tree Star). ILC2s (selected as $CD45^+/Lineage^-/Thy1.2^+/ST2^+$ cells) were sorted on an Influx cell sorter (BD) in the UVA flow cytometry core facility, achieving a purity of >90%.

RNA sequencing and analysis

ILC2s were FACs sorted, as described above, directly into lysis buffer (PicoPure RNA isolation kit; Applied Biosystems). RNA purification was performed according to manufacturer instructions and stored at −80°C until use. Library preparation, amplification, and RNA sequencing (Illumina) were performed by HudsonAlpha.

In vitro cell stimulation

For in vitro stimulation and cytokine staining of ILC2s, normalized numbers of cells were maintained in RPMI + 10% FBS + Anti-anti at 37°C. Cells were treated with Golgi block (Brefeldin A) and stimulated with PMA/ionomycin for 4 h before being washed and stained as described in the Flow cytometry/cell sorting section.

Image quantification

Images were acquired using an SP8 confocal microscope (Leica; fluorescence images) or a DMI 6000B widefield microscope (Leica; brightfield images). Counting was done in ImageJ (National Institutes of Health) with the "Cell Counter" plugin (Kurt De Vos, University of Sheffield, Sheffield, England, UK). Heat maps were generated with the "HeatMap Histogram" plugin (Samuel Péan).

To quantify spinal cord lesion size, 20-µm coronal sections were stained with GFAP and imaged. Lesion area per slice was quantified using ImageJ, and total volume was calculated using Excel (Microsoft).

Tissue preparation and immunofluorescence

For quantification of ILC2s, mice were perfused with heparinized (5 U/ml) PBS and 4% PFA, followed by meninges and spinal cord dissection. The tissue was postfixed for 48 h in 4% PFA, and spinal cords were cryoprotected in 30% sucrose for 48 h. Spinal cords were cut into 20-µm sections, mounted on gelatin-coated slides, and stored at −20°C until use. To stain, tissue was blocked for 1 h at room temperature in blocking buffer (2% serum [of the secondary's species]; 1% BSA; 0.1% triton; 0.05% tween; 0.05% Na Azide) followed by overnight incubation in primary antibody at 4°C. The following antibodies were used for immunofluorescence staining: chicken anti-GFAP (AB5541; 1:1,000; EMD Millipore), rat anti-CD3 660 (50-0032; 1:300; eBioscience), rat anti-CD3 biotin (13-0032; 1:300; eBioscience). Slices were washed 3× 10 min and incubated for 2 h at room temperature with the appropriate secondary antibodies (all from Thermo Fisher Scientific; 1:1,000), washed again 3 × 10 min and mounted with Aqua-Mount (Thermo Fisher Scientific) and DAPI.

experiments; Student's *t* test). (C) Flow cytometry analysis of IL-5 expression in ILC2s at 1DPI in spinal cord meninges (i; P = 0.624) and brain meninges (ii; P = 0.027; *n* = 3, representative of two experiments; Student's *t* test). (D) WT and IL-$33^{-/-}$ animals were injured, and meningeal ILC2s were analyzed for IL-13 expression 1DPI in spinal cord meninges (i; P = 0.358) and brain meninges (ii; P = 0.031; *n* = 4; Student's *t* test). (E) WT and IL-$33^{-/-}$ animals were injured, and meningeal ILC2s were analyzed for IL-5 expression 1DPI in spinal cord meninges (i; P = 0.753) and brain meninges (ii; P = 0.003; *n* = 4; Student's *t* test). (F–H) Uninjured and 1DPI brain meningeal ILC2 transcriptomes were analyzed by RNAseq. (F) Volcano plot of injured versus uninjured ILC2 gene expression. 305 genes were significantly altered between groups (*n* = 3, each sample five pooled mice; adjusted p-value <0.050). (G and H) Gene sets enriched among differentially expressed genes in injured versus meningeal ILC2s. Histogram (G) and heat maps (H) of select gene sets and their component genes (*n* = 3, each sample five pooled mice; adjusted p-value <0.050). Error bars represent mean ± SEM; *, P ≤ 0.05; **, P ≤ 0.01.

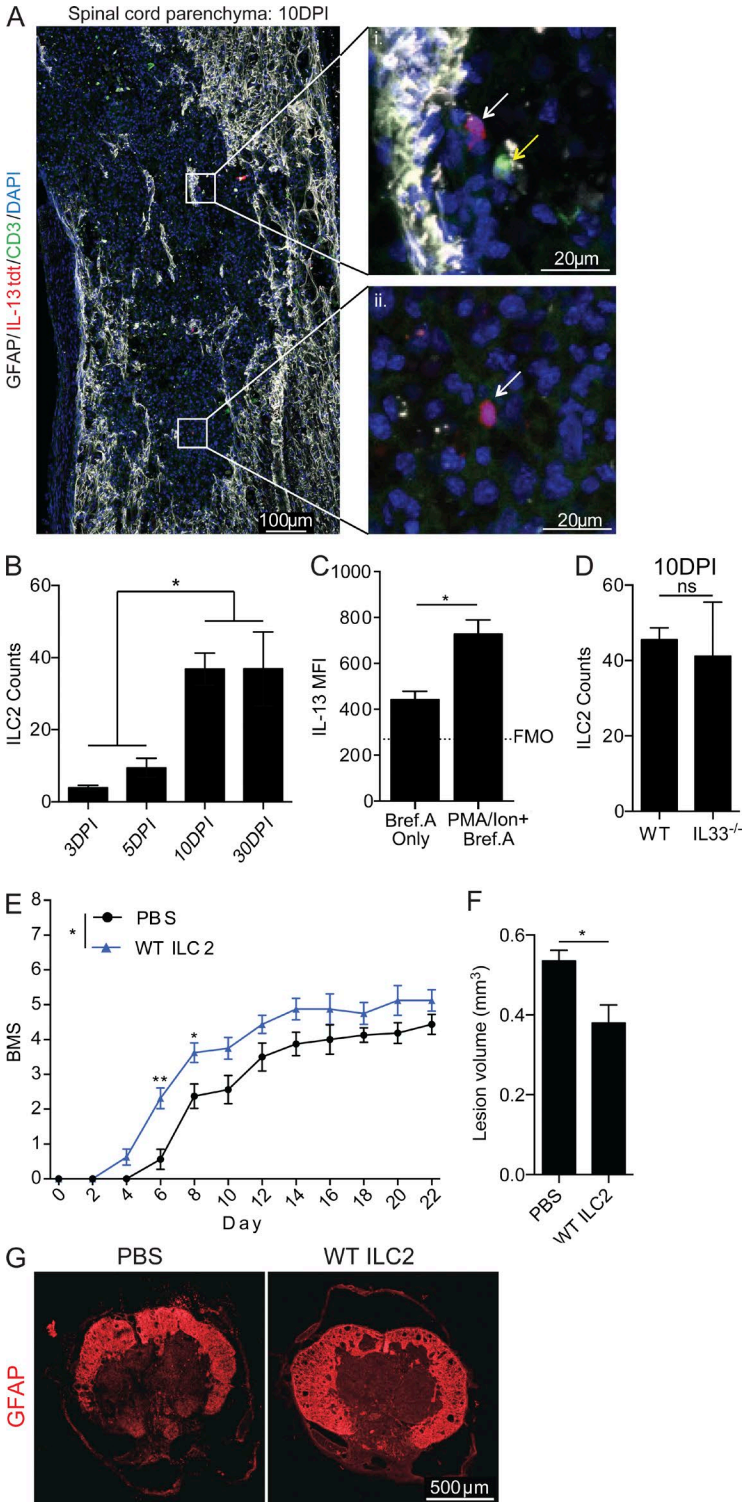

Figure 4. **Beneficial role of ILC2s in SCI.** (A) Immunofluorescent staining of IL-13^{tdt}+ ILC2s in the spinal cord 10 d after SCI. Insets show zoomed-in images of representative ILC2s (white arrows, IL-13^{tdt}+/CD3^{-}) or T cells (yellow arrows, IL-13^{tdt}−/CD3^{+}) in the injury site at 10DPI. (B) Time course of ILC2 infiltration into the SCI site measured by flow cytometry (3DPI vs. 10DPI P = 0.016, 3DPI vs. 30DPI P = 0.015, 5DPI vs. 10DPI P = 0.040, 5DPI vs. 30DPI P = 0.039; n = 3, representative of two experiments; one-way ANOVA with Tukey's multiple comparisons test). (C and D) Single-cell suspensions of SCI sites 10DPI were stimulated and assessed for IL-13 expression (C; P = 0.007; n = 4; Student's t test). (D) WT and IL-33$^{-/-}$ mice were injured, and at 10DPI, the injury site was analyzed for ILC2 infiltration (P = 0.741; n = 4 WT and 3 IL-33$^{-/-}$ mice; Student's t test). (E) FACS-isolated lung-derived ILC2s (5 × 10^3) from WT mice were delivered intracerebroventricularly (i.c.v.) into ST2$^{-/-}$ animals in 1 µl PBS the day before injury. The control group received 1 µl PBS i.c.v. (P = 0.017; n = 8; repeated measures two-way ANOVA with Šídák's multiple comparisons test). (F and G) Lesion volume was calculated on injured tissues 30DPI. (F) ILC2-treated mice had smaller lesions (P = 0.040; n = 4; Student's t test). (G) Representative coronal images of GFAP staining from the center of spinal cord lesions. Error bars represent mean ± SEM; *, P ≤ 0.05; **, P ≤ 0.01.

Toluidine blue staining

For staining meningeal mast cells, toluidine blue staining was performed on samples after being stained and imaged for fluorescence markers. Meninges were stained in 0.5% Toluidine blue O (pH 2.5; Sigma-Aldrich) for 15 min at room temperature. Toluidine blue was washed overnight at 4°C, and images were acquired using brightfield microscopy.

Spinal cord contusion

Female mice were first anesthetized with ketamine/xylazine. The back fur was shaved and underlying skin sterilized with an iodide/betadine solution. An incision was made over the T9-T10 vertebrae, and the skin was held back with retractors. The fascia overlying the spinal cord was removed to expose the vertebrae. The T10 vertebra was removed with fine rongeurs to expose the spinal cord. The IH-0400 Impactor (Precision Systems and Instrumentation) was used to contuse the spinal cord centrally, after which the muscles and skin overlying the spinal cord were sutured closed and the mouse was allowed to recover on warming pads. The force of impact was computer controlled and set to 70 or 90 KDyn as noted in the text/legends. Mice were maintained on sulfa water, and twice daily we performed manual bladder expulsion. Two blinded observers assessed recovery of hind-limb locomotor activity with the BMS (Basso et al., 2006) after injury.

IL-33 treatment

For IL-33 treatments to expand ILC2s, mice were injected i.p. with 500 ng carrier-free recombinant IL-33 (eBioscience) every other day. After three injections, mice were sacrificed, and ILC2 numbers were analyzed by flow cytometry.

RNAseq analysis

The raw sequencing reads (FASTQ files) went through two stages of preprocessing to remove low-quality reads and bases. First, they were chastity filtered, which removes any clusters that have a higher than expected intensity of the called base compared with other bases. Then they were trimmed with Trimmomatic (Bolger et al., 2014) to remove low-quality bases (minimum read length after trimming = 36). After preprocessing, the quality of the reads was evaluated using FastQC, and after passing quality control (QC), the reads were aligned to the UCSC mm9 genome (Harrow et al., 2012) using the splice-aware read aligner STAR (Dobin et al., 2013). The quality of the alignments was next assessed by SAMStat (Lassmann et al., 2011), and any low-quality alignments were removed with SAMtools (Li et al., 2009; MAPQ < 10). Next, the number of reads aligning to each gene was quantified with HTSeq (Anders et al., 2015), and then the Bioconductor package (Love et al., 2014) DESeq2 was used to normalize the raw counts and perform exploratory analysis (e.g., PCA) and differential expression analysis. The Benjamini–Hochberg false discovery rate procedure was used to correct the p-values for multiple testing. Heat maps of the differentially expressed genes generated with the R package pheatmap (https://CRAN.R-project.org/package=pheatmap). To compare the highly expressed genes in the uninjured lung versus uninjured brain meninges, the normalized, $\log_2$ transformed counts were converted to standard scores (z-score) using the *scale* function in R. The mean z-score for each gene was then calculated, and those with a z-score >1.5 (i.e., 1.5 standard deviations above the mean) were considered highly expressed. The UpSet plot (Lex et al., 2014) used to visualize the overlap between the uninjured lung and brain samples was created with the R package UpSetR (Gehlenborg, 2016). The R implementation of Fisher's exact test, *fisher.test*, was used to identify enriched gene sets in the differentially expressed genes using two gene set collections: the GO biological process from MSigDB (Subramanian et al., 2005; C5) and the gene families from the Hugo Gene Nomenclature Committee (HGNC; Gray et al., 2015).

Accession number

All sequencing data has been uploaded to the GEO repository under accession no. GSE90908.

Online supplemental material

Fig. S1 contains images of whole-mount IL-13^{tdt} meninges, demonstrating visually how ILC2s are concentrated in the dural sinus area. Fig. S2 contains data regarding the use of anti-Thy1.2 antibody to deplete ILC2s, demonstrating that, in our hands, it merely blocks the Thy1.2 epitope. Table S1 lists normalized gene expression values for all RNAseq samples (uninjured and injured meninges and uninjured lung ILC2s). Table S2 lists differential expression between uninjured meninges and lung ILC2s, as well as the gene sets enriched in lung ILC2s. Table S3 lists differential expression between uninjured and injured meninges ILC2s, as well as the gene sets enriched in injured meninges ILC2s. Tables S1–S3 are available as Excel files.

ACKNOWLEDGMENTS

We would like to thank all the members of the Kipnis laboratory for their valuable comments during multiple discussions of this work.

This work was supported by a grant from the National Institutes of Health (NS081026 to J. Kipnis).

The authors declare no competing financial interests.

Submitted: 26 November 2016
Revised: 9 December 2016
Accepted: 13 December 2016

REFERENCES

Ackery, A.D., M.D. Norenberg, and A. Krassioukov. 2007. Calcitonin gene-related peptide immunoreactivity in chronic human spinal cord injury. *Spinal Cord*. 45:678–686. http://dx.doi.org/10.1038/sj.sc.3102020

Anders, S., P.T. Pyl, and W. Huber. 2015. HTSeq—a Python framework to work with high-throughput sequencing data. *Bioinformatics*. 31:166–169. http://dx.doi.org/10.1093/bioinformatics/btu638

Aspelund, A., S. Antila, S.T. Proulx, T.V. Karlsen, S. Karaman, M. Detmar, H. Wiig, and K. Alitalo. 2015. A dural lymphatic vascular system that drains brain interstitial fluid and macromolecules. *J. Exp. Med*. 212:991–999. http://dx.doi.org/10.1084/jem.20142290

Basso, D.M., L.C. Fisher, A.J. Anderson, L.B. Jakeman, D.M. McTigue, and P.G. Popovich. 2006. Basso Mouse Scale for locomotion detects differences in recovery after spinal cord injury in five common mouse strains. *J. Neurotrauma*. 23:635–659. http://dx.doi.org/10.1089/neu.2006.23.635

Besnard, A.G., R. Guabiraba, W. Niedbala, J. Palomo, F. Reverchon, T.N. Shaw, K.N. Couper, B. Ryffel, and F.Y. Liew. 2015. IL-33-mediated protection against experimental cerebral malaria is linked to induction of type 2 innate lymphoid cells, M2 macrophages and regulatory T cells. *PLoS Pathog.* 11:e1004607. http://dx.doi.org/10.1371/journal.ppat.1004607

Blesch, A., and M.H. Tuszynski. 2001. GDNF gene delivery to injured adult CNS motor neurons promotes axonal growth, expression of the trophic neuropeptide CGRP, and cellular protection. *J. Comp. Neurol.* 436:399–410. http://dx.doi.org/10.1002/cne.1076

Bolger, A.M., M. Lohse, and B. Usadel. 2014. Trimmomatic: a flexible trimmer for Illumina sequence data. *Bioinformatics.* 30:2114–2120. http://dx.doi.org/10.1093/bioinformatics/btu170

Bracci-Laudiero, L., L. Aloe, M.C. Caroleo, P. Buanne, N. Costa, G. Starace, and T. Lundeberg. 2005. Endogenous NGF regulates CGRP expression in human monocytes, and affects HLA-DR and CD86 expression and IL-10 production. *Blood.* 106:3507–3514. http://dx.doi.org/10.1182/blood-2004-10-4055

Bulloch, K., T.A. Milner, A. Prasad, M. Hsu, G. Buzsaki, and B.S. McEwen. 1998. Induction of calcitonin gene-related peptide-like immunoreactivity in hippocampal neurons following ischemia: a putative regional modulator of the CNS injury/immune response. *Exp. Neurol.* 150:195–205. http://dx.doi.org/10.1006/exnr.1997.6765

Derecki, N.C., A.N. Cardani, C.H. Yang, K.M. Quinnies, A. Crihfield, K.R. Lynch, and J. Kipnis. 2010. Regulation of learning and memory by meningeal immunity: a key role for IL-4. *J. Exp. Med.* 207:1067–1080. http://dx.doi.org/10.1084/jem.20091419

Diem, R., M. Hobom, P. Grötsch, B. Kramer, and M. Bähr. 2003. Interleukin-1β protects neurons via the interleukin-1 (IL-1) receptor-mediated Akt pathway and by IL-1 receptor-independent decrease of transmembrane currents in vivo. *Mol. Cell. Neurosci.* 22:487–500. http://dx.doi.org/10.1016/S1044-7431(02)00042-8

Dobin, A., C.A. Davis, F. Schlesinger, J. Drenkow, C. Zaleski, S. Jha, P. Batut, M. Chaisson, and T.R. Gingeras. 2013. STAR: ultrafast universal RNA-seq aligner. *Bioinformatics.* 29:15–21. http://dx.doi.org/10.1093/bioinformatics/bts635

Dusart, I., and M.E. Schwab. 1994. Secondary cell death and the inflammatory reaction after dorsal hemisection of the rat spinal cord. *Eur. J. Neurosci.* 6:712–724. http://dx.doi.org/10.1111/j.1460-9568.1994.tb00983.x

Filiano, A.J., Y. Xu, N.J. Tustison, R.L. Marsh, W. Baker, I. Smirnov, C.C. Overall, S.P. Gadani, S.D. Turner, Z. Weng, et al. 2016. Unexpected role of interferon-γ in regulating neuronal connectivity and social behaviour. *Nature.* 535:425–429. http://dx.doi.org/10.1038/nature18626

Gadani, S.P., J.T. Walsh, J.R. Lukens, and J. Kipnis. 2015a. Dealing with danger in the CNS: The response of the immune system to injury. *Neuron.* 87:47–62. http://dx.doi.org/10.1016/j.neuron.2015.05.019

Gadani, S.P., J.T. Walsh, I. Smirnov, J. Zheng, and J. Kipnis. 2015b. The glia-derived alarmin IL-33 orchestrates the immune response and promotes recovery following CNS injury. *Neuron.* 85:703–709. http://dx.doi.org/10.1016/j.neuron.2015.01.013

Gehlenborg, N.2016. UpSetR: A More Scalable Alternative to Venn and Euler Diagrams for Visualizing Intersecting Sets. R package version 1.2.2. Available at: https://rdrr.io/cran/UpSetR/

Goldmann, T., P. Wieghofer, M.J. Jordão, F. Prutek, N. Hagemeyer, K. Frenzel, L. Amann, O. Staszewski, K. Kierdorf, M. Krueger, et al. 2016. Origin, fate and dynamics of macrophages at central nervous system interfaces. *Nat. Immunol.* 17:797–805. http://dx.doi.org/10.1038/ni.3423

Gorski, S.A., Y.S. Hahn, and T.J. Braciale. 2013. Group 2 innate lymphoid cell production of IL-5 is regulated by NKT cells during influenza virus infection. *PLoS Pathog.* 9:e1003615. http://dx.doi.org/10.1371/journal.ppat.1003615

Gray, K.A., B. Yates, R.L. Seal, M.W. Wright, and E.A. Bruford. 2015. Genenames.org: the HGNC resources in 2015. *Nucleic Acids Res.* 43:D1079–D1085. http://dx.doi.org/10.1093/nar/gku1071

Halim, T.Y. 2016. Group 2 innate lymphoid cells in disease. *Int. Immunol.* 28:13–22. http://dx.doi.org/10.1093/intimm/dxv050

Harrow, J., A. Frankish, J.M. Gonzalez, E. Tapanari, M. Diekhans, F. Kokocinski, B.L. Aken, D. Barrell, A. Zadissa, S. Searle, et al. 2012. GENCODE: the reference human genome annotation for The ENCODE Project. *Genome Res.* 22:1760–1774. http://dx.doi.org/10.1101/gr.135350.111

Kivisäkk, P., J. Imitola, S. Rasmussen, W. Elyaman, B. Zhu, R.M. Ransohoff, and S.J. Khoury. 2009. Localizing central nervous system immune surveillance: meningeal antigen-presenting cells activate T cells during experimental autoimmune encephalomyelitis. *Ann. Neurol.* 65:457–469. http://dx.doi.org/10.1002/ana.21379

Lassmann, T., Y. Hayashizaki, and C.O. Daub. 2011. SAMStat: monitoring biases in next generation sequencing data. *Bioinformatics.* 27:130–131. http://dx.doi.org/10.1093/bioinformatics/btq614

Lex, A., N. Gehlenborg, H. Strobelt, R. Vuillemot, and H. Pfister. 2014. UpSet: Visualization of Intersecting Sets. *IEEE Trans. Vis. Comput. Graph.* 20:1983–1992. http://dx.doi.org/10.1109/TVCG.2014.2346248

Li, H., B. Handsaker, A. Wysoker, T. Fennell, J. Ruan, N. Homer, G. Marth, G. Abecasis, and R. Durbin; 1000 Genome Project Data Processing Subgroup. 2009. The Sequence Alignment/Map format and SAMtools. *Bioinformatics.* 25:2078–2079. http://dx.doi.org/10.1093/bioinformatics/btp352

Louveau, A., I. Smirnov, T.J. Keyes, J.D. Eccles, S.J. Rouhani, J.D. Peske, N.C. Derecki, D. Castle, J.W. Mandell, K.S. Lee, et al. 2015. Structural and functional features of central nervous system lymphatic vessels. *Nature.* 523:337–341. http://dx.doi.org/10.1038/nature14432

Love, M.I., W. Huber, and S. Anders. 2014. Moderated estimation of fold change and dispersion for RNA-seq data with DESeq2. *Genome Biol.* 15:550. http://dx.doi.org/10.1186/s13059-014-0550-8

Molofsky, A.B., J.C. Nussbaum, H.E. Liang, S.J. Van Dyken, L.E. Cheng, A. Mohapatra, A. Chawla, and R.M. Locksley. 2013. Innate lymphoid type 2 cells sustain visceral adipose tissue eosinophils and alternatively activated macrophages. *J. Exp. Med.* 210:535–549. http://dx.doi.org/10.1084/jem.20121964

Monticelli, L.A., G.F. Sonnenberg, M.C. Abt, T. Alenghat, C.G. Ziegler, T.A. Doering, J.M. Angelosanto, B.J. Laidlaw, C.Y. Yang, T. Sathaliyawala, et al. 2011. Innate lymphoid cells promote lung-tissue homeostasis after infection with influenza virus. *Nat. Immunol.* 12:1045–1054. http://dx.doi.org/10.1038/ni.2131

Moro, K., T. Yamada, M. Tanabe, T. Takeuchi, T. Ikawa, H. Kawamoto, J. Furusawa, M. Ohtani, H. Fujii, and S. Koyasu. 2010. Innate production of T_H2 cytokines by adipose tissue-associated c-Kit$^+$Sca-1$^+$ lymphoid cells. *Nature.* 463:540–544. http://dx.doi.org/10.1038/nature08636

Neill, D.R., S.H. Wong, A. Bellosi, R.J. Flynn, M. Daly, T.K. Langford, C. Bucks, C.M. Kane, P.G. Fallon, R. Pannell, et al. 2010. Nuocytes represent a new innate effector leukocyte that mediates type-2 immunity. *Nature.* 464:1367–1370. http://dx.doi.org/10.1038/nature08900

Odegaard, J.I., M.W. Lee, Y. Sogawa, A.M. Bertholet, R.M. Locksley, D.E. Weinberg, Y. Kirichok, R.C. Deo, and A. Chawla. 2016. Perinatal licensing of thermogenesis by IL-33 and ST2. *Cell.* 166:841–854. http://dx.doi.org/10.1016/j.cell.2016.06.040

Price, A.E., H.E. Liang, B.M. Sullivan, R.L. Reinhardt, C.J. Eisley, D.J. Erle, and R.M. Locksley. 2010. Systemically dispersed innate IL-13-expressing cells in type 2 immunity. *Proc. Natl. Acad. Sci. USA.* 107:11489–11494. http://dx.doi.org/10.1073/pnas.1003988107

Radjavi, A., I. Smirnov, N. Derecki, and J. Kipnis. 2014. Dynamics of the meningeal CD4$^+$ T-cell repertoire are defined by the cervical lymph nodes and facilitate cognitive task performance in mice. *Mol. Psychiatry.* 19:531–532. http://dx.doi.org/10.1038/mp.2013.79

Rak, G.D., L.C. Osborne, M.C. Siracusa, B.S. Kim, K. Wang, A. Bayat, D. Artis, and S.W. Volk. 2016. IL-33-dependent group 2 innate lymphoid cells promote cutaneous wound healing. *J. Invest. Dermatol.* 136:487–496. http://dx.doi.org/10.1038/JID.2015.406

Russi, A.E., M.E. Walker-Caulfield, M.E. Ebel, and M.A. Brown. 2015. Cutting edge: c-Kit signaling differentially regulates type 2 innate lymphoid cell accumulation and susceptibility to central nervous system

demyelination in male and female SJL mice. *J. Immunol.* 194:5609–5613. http://dx.doi.org/10.4049/jimmunol.1500068

Russo, A.F. 2015. Calcitonin gene-related peptide (CGRP): a new target for migraine. *Annu. Rev. Pharmacol. Toxicol.* 55:533–552. http://dx.doi.org/10.1146/annurev-pharmtox-010814-124701

Saenz, S.A., M.C. Siracusa, L.A. Monticelli, C.G. Ziegler, B.S. Kim, J.R. Brestoff, L.W. Peterson, E.J. Wherry, A.W. Goldrath, A. Bhandoola, and D. Artis. 2013. IL-25 simultaneously elicits distinct populations of innate lymphoid cells and multipotent progenitor type 2 (MPPtype2) cells. *J. Exp. Med.* 210:1823–1837. http://dx.doi.org/10.1084/jem.20122332

Shechter, R., A. London, C. Varol, C. Raposo, M. Cusimano, G. Yovel, A. Rolls, M. Mack, S. Pluchino, G. Martino, et al. 2009. Infiltrating blood-derived macrophages are vital cells playing an anti-inflammatory role in recovery from spinal cord injury in mice. *PLoS Med.* 6:e1000113. http://dx.doi.org/10.1371/journal.pmed.1000113

Subramanian, A., P. Tamayo, V.K. Mootha, S. Mukherjee, B.L. Ebert, M.A. Gillette, A. Paulovich, S.L. Pomeroy, T.R. Golub, E.S. Lander, and J.P. Mesirov. 2005. Gene set enrichment analysis: a knowledge-based approach for interpreting genome-wide expression profiles. *Proc. Natl. Acad. Sci. USA.* 102:15545–15550. http://dx.doi.org/10.1073/pnas.0506580102

Sun, Y., K. Jin, L. Xie, J. Childs, X.O. Mao, A. Logvinova, and D.A. Greenberg. 2003. VEGF-induced neuroprotection, neurogenesis, and angiogenesis after focal cerebral ischemia. *J. Clin. Invest.* 111:1843–1851. http://dx.doi.org/10.1172/JCI200317977

Talbot, S., R.E. Abdulnour, P.R. Burkett, S. Lee, S.J. Cronin, M.A. Pascal, C. Laedermann, S.L. Foster, J.V. Tran, N. Lai, et al. 2015. Silencing nociceptor neurons reduces allergic airway inflammation. *Neuron.* 87:341–354. http://dx.doi.org/10.1016/j.neuron.2015.06.007

Toth, C.C., D. Willis, J.L. Twiss, S. Walsh, J.A. Martinez, W.Q. Liu, R. Midha, and D.W. Zochodne. 2009. Locally synthesized calcitonin gene-related Peptide has a critical role in peripheral nerve regeneration. *J. Neuropathol. Exp. Neurol.* 68:326–337. http://dx.doi.org/10.1097/NEN.0b013e31819ac71b

Van Dyken, S.J., A. Mohapatra, J.C. Nussbaum, A.B. Molofsky, E.E. Thornton, S.F. Ziegler, A.N. McKenzie, M.F. Krummel, H.E. Liang, and R.M. Locksley. 2014. Chitin activates parallel immune modules that direct distinct inflammatory responses via innate lymphoid type 2 and γδ T cells. *Immunity.* 40:414–424. http://dx.doi.org/10.1016/j.immuni.2014.02.003

Walsh, J.T., S. Hendrix, F. Boato, I. Smirnov, J. Zheng, J.R. Lukens, S. Gadani, D. Hechler, G. Gölz, K. Rosenberger, et al. 2015. MHCII-independent $CD4^+$ T cells protect injured CNS neurons via IL-4. *J. Clin. Invest.* 125:699–714. (published erratum appears in *J. Clin. Invest.* 2015. 125:2547) http://dx.doi.org/10.1172/JCI82458

Zhan, L., L. Zheng, T. Hosoi, Y. Okuma, and Y. Nomura. 2015. Stress-induced neuroprotective effects of epiregulin and amphiregulin. *PLoS One.* 10:e0118280. http://dx.doi.org/10.1371/journal.pone.0118280